Preferential oxidation of CO over Au/CuO_x-CeO_2 catalyst in microstructured reactors studied through CFD simulations

I. Uriz[a], G. Arzamendi[a], P.M. Diéguez[a], O.H. Laguna[b], M.A. Centeno[b], J.A. Odriozola[b], L.M. Gandía[a,*]

[a] *Departamento de Química Aplicada, Edificio de los Acebos, Universidad Pública de Navarra, Campus de Arrosadía s/n, E-31006 Pamplona, Spain*

[b] *Instituto de Ciencia de Materiales de Sevilla, Centro Mixto CSIC-Universidad de Sevilla, Avda. Américo Vespucio 49, 41092 Sevilla, Spain*

[*] Corresponding author. Phone: +34-948-169605. Fax: +34-948-169606.

E-mail address: lgandia@unavarra.es (Luis M. Gandía)

Abstract

…

Keywords: Catalytic wall reactor; CO preferential oxidation (CO-PrOx); Computational Fluid Dynamics (CFD); Microreactor; Microstructured reactor.

1. Introduction

A variety of hydrocarbons and alcohol fuels such as natural gas, biogas, bio-oil, diesel, bioethanol or glycerin may be reformed to a product gas known as reformate mainly containing hydrogen and a mixture of carbon oxides. Additional separation and purification steps are required to produce high-purity hydrogen. This is a critical issue if hydrogen will be used for feeding low-temperature fuel cells, such as the polymer-electrolyte-membrane fuel cells (PEMFC). In this case, hydrogen of 99.99999 % purity is required [1]. Reducing the content of CO is particularly important for this application because low-temperature PEMFC anodes are poisoned by this compound. Using some Pt-based alloys as the anode, the tolerance to CO in the hydrogen fuel may be increased from a few ppm to values between 50 and 100 ppm [2]. These extremely low CO levels cannot be reached through the water-gas shift (WGS) reaction which allows reducing the CO concentration to 0.5-1 vol. % at best. Among the several technologies available for further decreasing the CO content, the preferential CO oxidation (CO-PROX) is very well-suited for implementation in small-scale and compact fuel processors [2-4].

Microreactors and microtechnology is rapidly gaining interest in the entire energy field from portable and mobile power generation to stationary and decentralized production of fuels and electric power. Auxiliary power units based on fuel cells constitute a well-known example [5-7]. The first process involved in these energy systems is frequently the reforming of a fuel of convenience in microstructured reactors containing a heterogeneous catalyst in the form of a coating or a fixed-bed of very small particles. As concerns the fine removal of the CO present in the reformate stream, using CO-PROX is most frequent for systems of the smallest scale, *i.e.* of a power below 20 kW_e [8]. Kolb has recently reviewed the use of

microstructured reactors for decentralized and mobile fuel processing as hydrogen source for fuel cells. The catalytic CO-PROX in microreactors was also reviewed by Kolb [8]. The process is characterized by the strong exothermicity of the CO and H_2 oxidation reactions; for this reason, the control of the temperature becomes critical. On the other hand, it is frequently found that a significantly high oxygen-to-CO molar ratio ($\lambda = O/CO = 2O_2/CO$) in the reactor feed stream is required with respect to the stoichiometric one ($\lambda = 1$) to guarantee a suitable reduction of the CO content. Values of λ above 1.5 up to 4 and even 8 can be found in the literature. As a result of the combined effect of the several influencing parameters and the catalyst activity and selectivity, an operating temperatures window for optimal CO-PROX can be normally established. A wide window around a temperature close to a value suitable for feeding the fuel cell is in principle the most convenient situation. In view of the features of the CO-PROX process, the use of microreactors or microstructured reactors is particularly appealing due to their potential for achieving very high mass and heat transfer rates and relatively easy thermal integration.

A variety of catalysts have exhibited good performance for the CO-PROX reaction. They can be classified into noble metals (Pt, Rh, Ru), gold, and transition metals oxides catalysts [9,10]. In the case of microstructured reactors the catalysts most frequently used are the noble metals-based ones and specially the Pt catalysts. In this regard, Pt on Al_2O_3 [11-13], Al_2O_3-CeO_2 [14], and zeolite [15], Pt-Ru on α-Al_2O_3 [16], Pt-Rh on Al_2O_3 and CeO_2/SiO_2 [17,18], Pt-Co on Al_2O_3 [19,20], and Rh on Al_2O_3 and CeO_2 [21] have been considered in several studies. Among the transition metals oxides, copper oxides, and specially copper on ceria (CuO_x/CeO_2) catalysts have been the most widely investigated due to their good performance combining high activity and selectivity at relatively low reaction temperatures (< 280°C) [22-28]. Regarding gold, CeO_2 and α-Fe_2O_3 [29], α-Fe_2O_3-γ-Al_2O_3 [30] and TiO_2 [31] have been used as catalyst supports of this metal in microstructured reactors.

In previous studies by our group, a kinetic model for the CO-PROX reaction over a Cu-Ce oxide (10 wt. % CuO) was formulated. The kinetic model was implemented in a computational fluid dynamics (CFD) code of a microchannel reactor [32]. This model was satisfactorily validated against experimental data in a subsequent study in which the CuO_x-CeO_2 catalyst was coated onto the channels walls (5.46 $mg_{cat.}/cm^2$) of a microreactor block made of Al-alloyed ferritic stainless steel (Fecralloy®). The results showed that the CO content of a surrogate reformate stream containing 1 vol. % CO could be reduced to 20-40 ppm at the CO-PROX reactor outlet working within the 180-220 ºC range of temperature, $\lambda = 4$, and space time of 1 l (STP)/($g_{cat.}$·min). With the aim of improving the performance of the CuO_x-CeO_2 solid, 1 wt. % Au was incorporated by deposition-precipitation method to give the Au/CuO_x-CeO_2 catalyst. The kinetics of the CO-PROX reaction over the gold catalyst in powder form has been investigated in a preceding paper [33]. In the present paper, a parametric analysis of the CO-PROX reaction over the Au/CuO_x-CeO_2 catalyst in a microchannel reactor is performed through CFD simulations. The aim of this work is to evaluate the potential of the Au/CuO_x-CeO_2 catalyst comparing its performance with that of the copper-cerium oxide as a previous step to depositing it in a microchannel reactor.

2. Kinetic and CFD models

The kinetic model of the CO-PROX over the Au/CuO_x-CeO_2 catalyst includes rate expressions for the oxidation of CO (Eq. 1), oxidation of H_2 (Eq. 2) and the reverse water-gas shift (RWGS, Eq. 3) reactions:

$$CO + \frac{1}{2}O_2 \xrightarrow{k_{CO}} CO_2 \quad (1)$$

$$H_2 + \frac{1}{2}O_2 \xrightarrow{k_{H2}} H_2O \quad (2)$$

$$CO_2 + H_2 \xleftarrow{k_{RWGS}, K_{RWGS}} CO + H_2O \quad (3)$$

Rate equations for these reactions are as follows [33]:

$$-R_{CO} = \frac{k_{CO} \cdot P_{CO} \cdot P_{O_2}^{0.5}}{\left(1 + K_{CO_2} \cdot P_{CO_2} + K_{O_2} \cdot P_{O_2}^{0.5}\right)^2} \quad (4)$$

$$-R_{H_2} = k_{H_2} \cdot P_{H_2} \cdot P_{O_2}^{0.5} \quad (5)$$

$$-R_{RWGS} = k_{RWGS} \cdot \left(P_{CO_2} \cdot P_{H_2} - K_{WGS} \cdot P_{CO} \cdot P_{H_2O}\right) \quad (6)$$

where P_i (i = H_2, O_2, CO, CO_2, H_2O) are the corresponding partial pressures, k_j (j = CO, H_2, RWGS) the kinetic constants, K_{CO_2}, K_{O_2} the equilibrium constant for CO_2 and oxygen adsorption, respectively, and K_{WGS} the equilibrium constant of the water-gas shift reaction. Kinetic and adsorption constants were reparametrized as follows to improve numerical stability:

$$k_j = k_j^{ref} \cdot \exp\left(\frac{-E_j}{R}\left(\frac{1}{T} - \frac{1}{T^{ref}}\right)\right) \qquad ; T^{ref} = 373K \quad (7)$$

$$K_j = K_j^{ref} \cdot \exp\left(\frac{-\Delta H_j}{R}\left(\frac{1}{T} - \frac{1}{T^{ref}}\right)\right) \qquad ; T^{ref} = 373K \quad (8)$$

where E_j is the activation energy, ΔH_j the enthalpy of adsorption, T^{ref} an arbitrary reference temperature that was taken as 373 K, and k_j^{ref} and K_j^{ref} the kinetic and adsorption constants at the reference temperature, respectively. Kinetic parameters included in Eqs. 7 and 8 are given in Table 1. As concerns the CuO_x-CeO_2 oxide, the kinetic model for the CO-PROX reaction was reported elsewhere [32].

Three-dimensional (3D) simulations have been carried out with the commercial CFD software package ANSYS® CFX on a Lenovo dual-processor Intel® Xenon® ThinkStation D20 workstation running MS Windows 7 Professional® × 64 with an available RAM of

64.0 GB. Physical models consisted in square parallel microchannels of 20 mm of length and side *d* made of stainless steel. These models have been described in previous works by our group [34-37]. The effect of the characteristic dimension on the microreactor performance has been investigated. To this end, values of *d* of 0.35, 0.70, 1.4 and 2.8 mm have been considered. In addition, a geometry consisting in semicircular microchannels of radium (*R*) of 0.3, 0.6 and 1.2 mm have been also investigated. The computational domains were divided into meshes with control volumes where the governing equations are solved through iterative numerical methods until the established criteria of convergence are fulfilled. Two-dimensional meshes were constructed first, and then, they were extruded along the appropriate axis. In this way, the whole computational domain is as orthogonal as possible to reduce the truncation errors and computation time. This type of structured meshes is convenient when using first order upwind differencing discretization schemes, such as in the present study. Stretched grids were developed near the walls where the most pronounced changes of the transport properties can be expected. Mesh independence tests were performed to ensure that the solutions do not vary with the number of computational elements. Criteria of convergence were based on the residuals defined as the normalized root mean square (RMS) of the difference between the latest solution and the running arithmetic average of the variables. Under these conditions and with the grids adopted in this work, the imbalance level of the conservation equations after convergence was typically below 0.1 %.

CFD simulations have been conducted at steady state and atmospheric pressure. Catalytic reactions were modeled considering the microchannels walls as sources of products and sinks of reactants [34-37]. The kinetic model formed by Eqs. 1-8 were implemented in the CFD code. It has been assumed that a thin layer of the Au/CuO_x-CeO_2 catalyst was uniformly deposited onto the walls of the microreactors at loadings of 1, 2 and 5 mg/cm^2. Regarding the feed stream it has been considered that the oxygen is introduced with air. Its molar

composition for the base case was set at 69.5 % H_2, 10 % CO_2, 10 % H_2O, 1 % CO, 2 % O_2 (λ = 4), and 7.5 % N_2. It should be noted that a significant content of both CO_2 and H_2O has been considered to simulate a reformate off-gas after the WGS reactors. In order to study the effect of the O_2/CO molar ratio, values of the O_2 concentration of 1 (λ = 2) and 3 vol. % (λ = 6) have been also considered. Gas-hourly space velocities (GHSV) of 10 000, 18 000 and 50 000 h^{-1} (STP) have been used in the simulations.

CFD calculations including chemical kinetics are very demanding from the point of view of computing power. For this reason, a first series of simulations were performed under isothermal conditions (the energy transport equation should not be solved) to compare the performance of the Au/CuO_x-CeO_2 and CuO_x-CeO_2 catalysts, and study the effect of the main operating variables (reaction temperature, GHSV, catalyst loading, λ, characteristic dimension and microchannel geometry) on the CO-PROX process. Subsequently, a second series of simulations was performed including cooling of the CO-PROX microchannels with a stream of nitrogen and hydrogen that emulates the anode off-gas of a PEMFC.

3. Isothermal simulations

3.1. Comparison between Au/CuO_x-CeO_2 and CuO_x-CeO_2 under the base case CO-PROX

Fig. 1A-1D shows the performance of both the Au/CuO_x-CeO_2 (Au/CeCu) and CuO_x-CeO_2 (CeCu) catalysts under the base case feed stream molar composition (1 % CO, 2 % O_2, λ = 4), catalyst loading of 1 mg/cm^2, GHSV of 10 000 h^{-1}, and isothermal conditions. Simulations correspond to the CO-PROX reaction in square microchannels of d = 0.7 mm. It can be seen that the deposition of gold onto CuO_x-CeO_2 improves the catalytic activity because the oxygen (Fig. 1B) and CO (Fig. 1C) conversions become complete at 184 ºC over

Au/CuO_x-CeO_2 whereas a temperature of about 200 ºC is required for complete conversion over CuO_x-CeO_2. However, for a given reaction temperature, the hydrogen conversion (Fig. 1D) is also higher over the gold catalyst. Moreover, the increase of the hydrogen conversion is higher than that of CO resulting in a lower selectivity to CO oxidation over Au/CuO_x-CeO_2 compared with CuO_x-CeO_2. As a consequence, the minimum CO content at the reactor outlet (Fig. 1A) is higher for Au/CuO_x-CeO_2 (55 ppm) than for CuO_x-CeO_2 (7 ppm). The minimum CO contents are obtained at the temperatures at which 100 % oxygen conversion is reached. For temperatures above this value the oxidation of hydrogen becomes more favored than that of CO so the CO concentration at the microchannels outlet starts to increase (Fig. 1A).

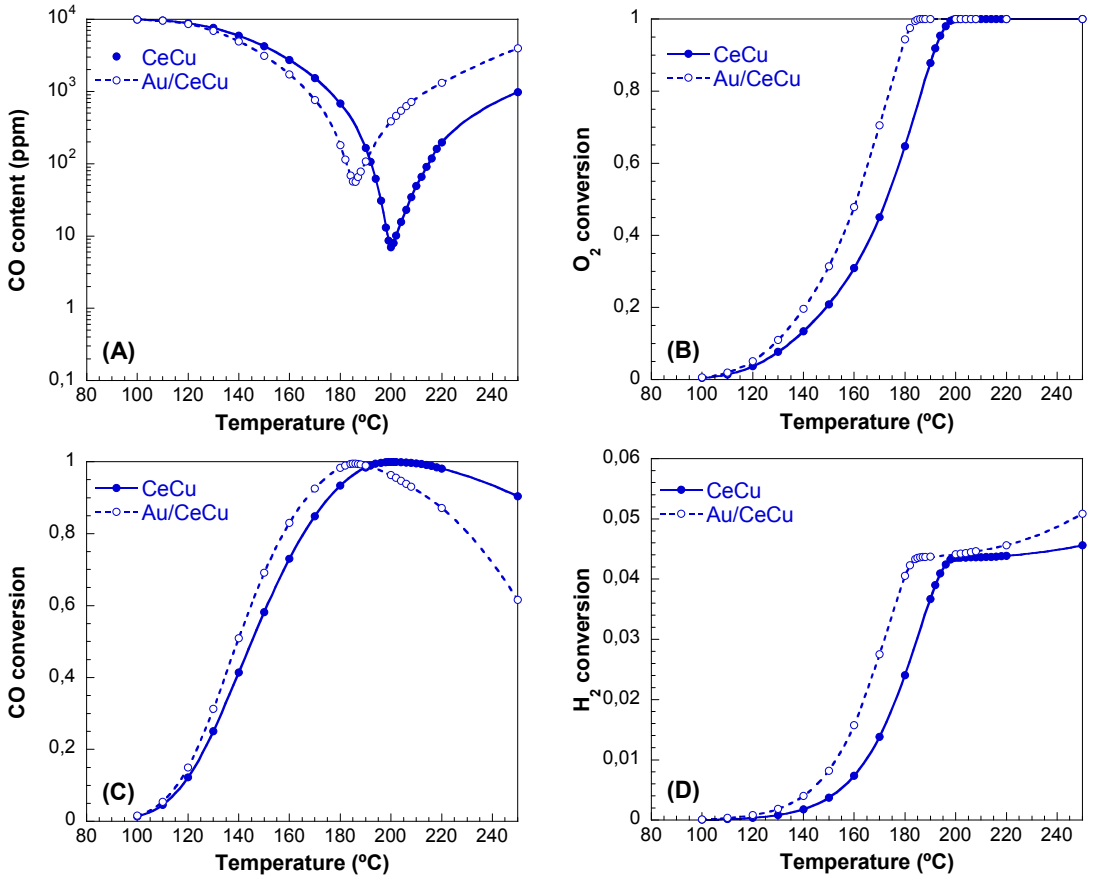

Fig. 1. Evolution of the mean CO content (A), O_2 conversion (B), CO conversion (C) and H_2 conversion (D) at the microchannels (d = 0.7 mm) outlet as a function of the reaction temperature for the base case CO-PROX over the catalysts indicated. GHSV=10 000 h^{-1}, 1 vol. % CO, $\lambda = 4$, and catalyst loading of 1 mg/cm^2.

The hydrogen conversion at the temperatures that guarantee the minimum CO content is very similar for both catalysts, about 4.4 %. This a direct measurement of the hydrogen lost during the CO clean-up process.

Taking 100 ppm as the allowable limit for the CO concentration for the reformate stream at the exit of the CO-PROX reactor, the operating temperature becomes narrower after the incorporation of gold. According to Fig. 1A, under the simulation conditions of the base case, the temperature window for Au/CuO_x-CeO_2 covers only 8 ºC, from 182 to 190 ºC, whereas for CuO_x-CeO_2 the temperatures window widens to 23 ºC, from 192 to 215 ºC.

3.2. Influence of the operating parameters

In this section, the influence of the oxygen-to-CO ratio (λ), catalyst loading, and GHSV on the performance of microchannel reactors coated with the Au/CuO_x-CeO_2 and CuO_x-CeO_2 catalysts is examined. The CFD simulations were performed under isothermal conditions for square microchannels of d = 0.7 mm and a reformate stream containing 1 vol. % H_2 and 10 vol. % of both CO_2 and H_2O. Regarding the influence of λ, as oxygen is fed with air, the increase of λ implies the increase of the concentration of both O_2 and N_2. As a consequence, the concentration of H_2 has been suitably adjusted for each value of λ in order to keep the concentrations of CO, CO_2 and H_2O constant. The hydrogen concentrations were 74.2 vol. % for λ = 2, 69.5 vol. % for λ = 4, and 64.7 vol. % for λ = 6.

According to Fig. 2A, the CO content at the microreactor outlet decreases as the excess of oxygen in the feed stream increases with respect to the stoichiometric value. The change is significant when passing from λ = 2 to 4. In such a case, the final CO content decreases from 199 to 55 ppm in the case of the gold catalyst and from 23 to 7 ppm in the case of the CuO_x-CeO_2 oxide. As shown in Fig. 2B, this gain in CO removal efficiency is at the expense of

increased hydrogen losses because, for both catalysts, the conversion of hydrogen increases from about 1.4 % to 4.4 % when λ increases from 2 to 4. A further increase of λ up to 6 leads to 35 ppm of CO at the exit of the microreactor loaded with the Au/CuO_x-CeO_2, and 5 ppm CO in the cases of the microreactor containing CuO_x-CeO_2. It is difficult, especially for the oxide catalyst, that this additional reduction of the CO content can compensate for the further loss of hydrogen, whose conversion increases from 4.4 % to 7.7 % (Fig. 2B).

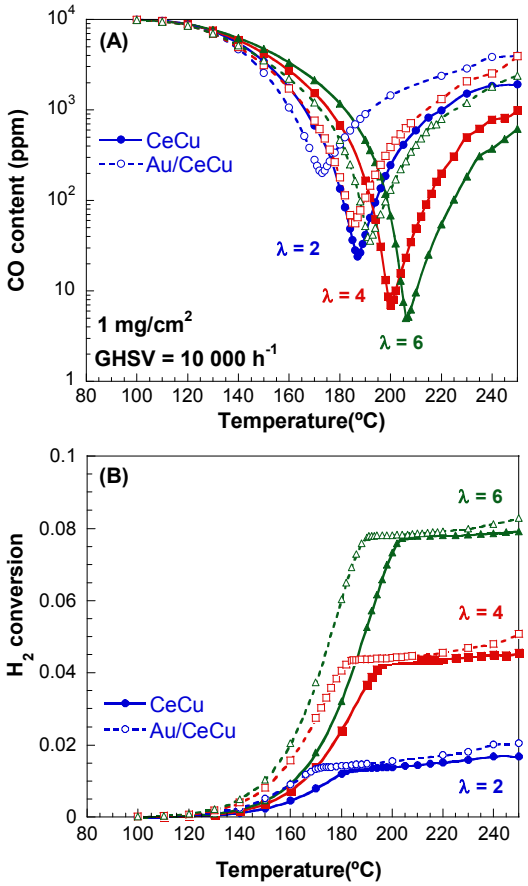

Fig. 2. Evolution of the mean CO content (A) and the hydrogen conversion (B) at the microchannels (d = 0.7 mm) outlet as a function of the reaction temperature and the oxygen-to-CO ratio. GHSV = 10 000 h^{-1}, catalyst loading of 1 mg/cm^2. Open symbols: Au/CuO_x-CeO_2 catalyst; filled symbols: CuO_x-CeO_2 catalyst.

Another interesting feature of the influence of the oxygen concentration excess is that achieving the minimum CO concentration in the reformate requires increasingly higher CO-PROX temperatures as λ increases. Regarding the gold catalyst, the minimum concentration

of CO is achieved at 173, 184 and 192 ºC when λ increases from 2 to 4 and 6, respectively. A similar increase takes place for CuO_x-CeO_2: from 187 to 199 and 206 ºC. The change of the feed stream concentration as λ increases has similar impacts on the rates of CO and H_2 oxidation. Whereas both rates increase with the concentration of oxygen as $P_{O_2}^{0.5}$, there are factors that soften this effect. Indeed, the partial pressure of O_2 is also present in the adsorption term of the CO oxidation rate (Eq. 4) and, as explained before, the concentration of H_2 in the feed has been lowered as λ increases which affects the hydrogen oxidation rate (Eq. 5). Taking into account that the minimum CO concentration corresponds to the temperature at which 100 % oxygen conversion is achieved (see Section 3.1), the increase of this temperature with λ can be mainly attributed to the increased concentration of oxygen that should be consumed to reach that point.

The effect of the catalyst loading and GHSV on the CO content at the microreactors outlet for λ = 4 is shown in Figs. 3A and 3B, respectively. As for the catalyst loading, values of 1, 2 and 5 mg/cm^2 at GHSV of 10 000 h^{-1} have been considered. To give an idea, a loading of 5.46 mg/cm^2 is easily achievable and has been used in our previous works with CuO_x-CeO_2 coated microchannel reactors [26,28]. As expected, the CO content of the reformate decreases as the catalyst loading increases. The temperature at which the minimum CO content is reached decreases as well (Fig. 3A). Regarding the gold catalyst, whereas a low loading of 1 mg/cm^2 allowed a relatively modest reduction of the CO concentration to 55 ppm, increasing the loading up to 2 and 5 mg/cm^2 decreases the final CO content to very interesting values from the practical point of view of 10 ppm (175 ºC) and 1.7 ppm (162 ºC), respectively. In the case of the CuO_x-CeO_2 oxide, the loadings of 2 and 5 mg/cm^2 allow decreasing the CO concentration at the microreactor outlet at levels below 1 ppm (190 ºC) in accordance with the higher selectivity of this catalyst.

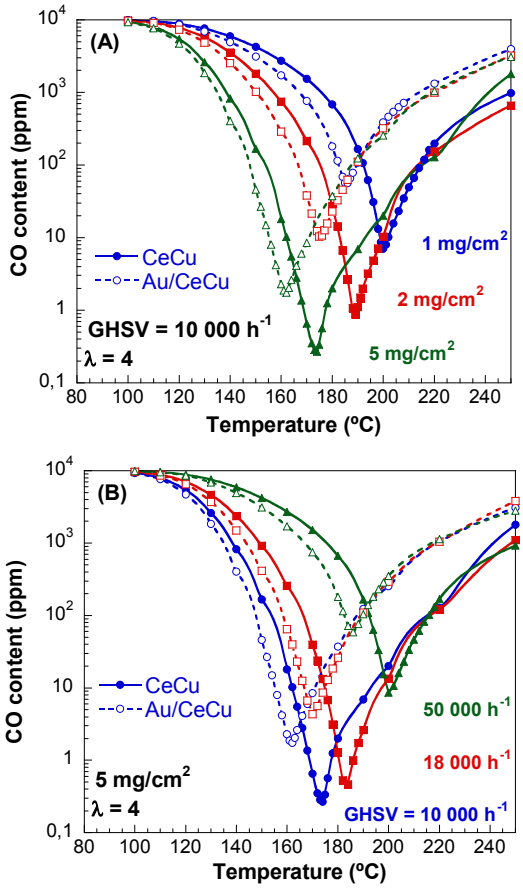

Fig. 3. Evolution of the mean CO content at the microchannels (d = 0.7 mm) outlet as a function of the reaction temperature and the catalyst loading (A) and GHSV (B). λ = 4. Open symbols: Au/CuO_x-CeO_2 catalyst; filled symbols: CuO_x-CeO_2 catalyst.

The space velocity is an important parameter as concerns process intensification. An example of the benefits of using microreactors for fully exploiting the potential of catalysts is given by Fig. 3B. It can be seen that the microreactor coated with CuO_x-CeO_2 (5 mg/cm^2) is capable of maintaining the minimum CO exit concentration below 10 ppm at GHSV values as high as 50 000 h^{-1}. Moreover, this is achieved at reaction temperatures not above 200 ºC. In the case of the gold catalyst (5 mg/cm^2), the minimum final CO concentration is kept below 5 ppm for space velocities up to 18 000 h^{-1}. At GHSV of 50 000 h^{-1} the CO content of the reformate under optimal temperature conditions (186 ºC) decreases to 57 ppm, a value that can be tolerated by PEMFC anodes made of Pt-Ru alloys [2]. As far as λ = 4 and the

temperature is below the optimum value, the hydrogen conversion is limited to 4.4 % in the simulations included in Fig. 3.

3.3. Influence of the CO_2 content of the reformate

It is well-known, and evident from Eq. 4, that the presence of CO_2 in the reformate has a negative effect on the rate of CO oxidation, and hence on the CO-PROX process. As shown in Fig. 4 for the Au/CuO_x-CeO_2 catalyst, the consequence is that the CO content of the reformate stream at the microreactor exit increases as the CO_2 content of the feed stream also increases. In these simulations, the concentration of H_2, CO, O_2 and H_2O were kept constant at 70, 1, 1 and 4 vol. %, respectively. The CO_2 concentration was varied between 5 and 20 vol. % and the balance corresponded to N_2. The concentration of CO_2 greatly influences the microreactor performance so this variable should be carefully controlled. Whereas the optimum temperature at which the minimum CO concentration is reached does not change, the minimum CO content increases from 10 to, 60, 187 and 390 ppm on varying the CO_2 concentration from 5 to 10, 15 and finally 20 vol. %.

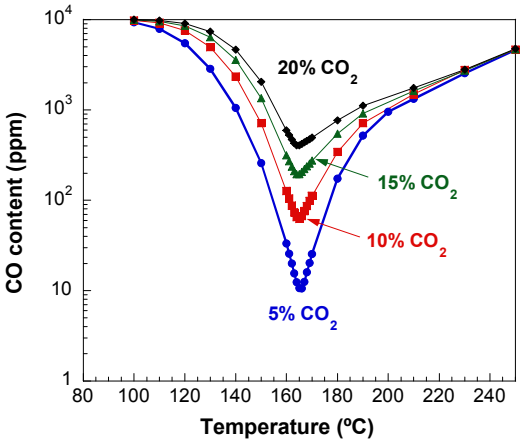

Fig. 4. Evolution of the mean CO content at the microchannels (d = 0.7 mm) outlet as a function of the reaction temperature and the CO_2 concentration for the microreactor coated with the Au/CuO_x-CeO_2 catalyst (2 mg/cm^2). GHSV=10 000 h^{-1}, λ = 2.

3.4. Influence of the microchannel characteristic size and shape

Fig 5 shows the influence of the characteristic dimension on the performance of microchannels for the CO-PROX process. In addition to the square microchannels, semicircular channels have been also considered. Whereas the square channels are normally fabricated by micromilling, the semicircular shape is typically obtained when chemical etching is used to fabricate the microducts. The characteristic dimension (d), or hydraulic diameter, of the square channels is the square side. For the semicircular channel, obviously, $d = 2R$, being R the semicircle radius.

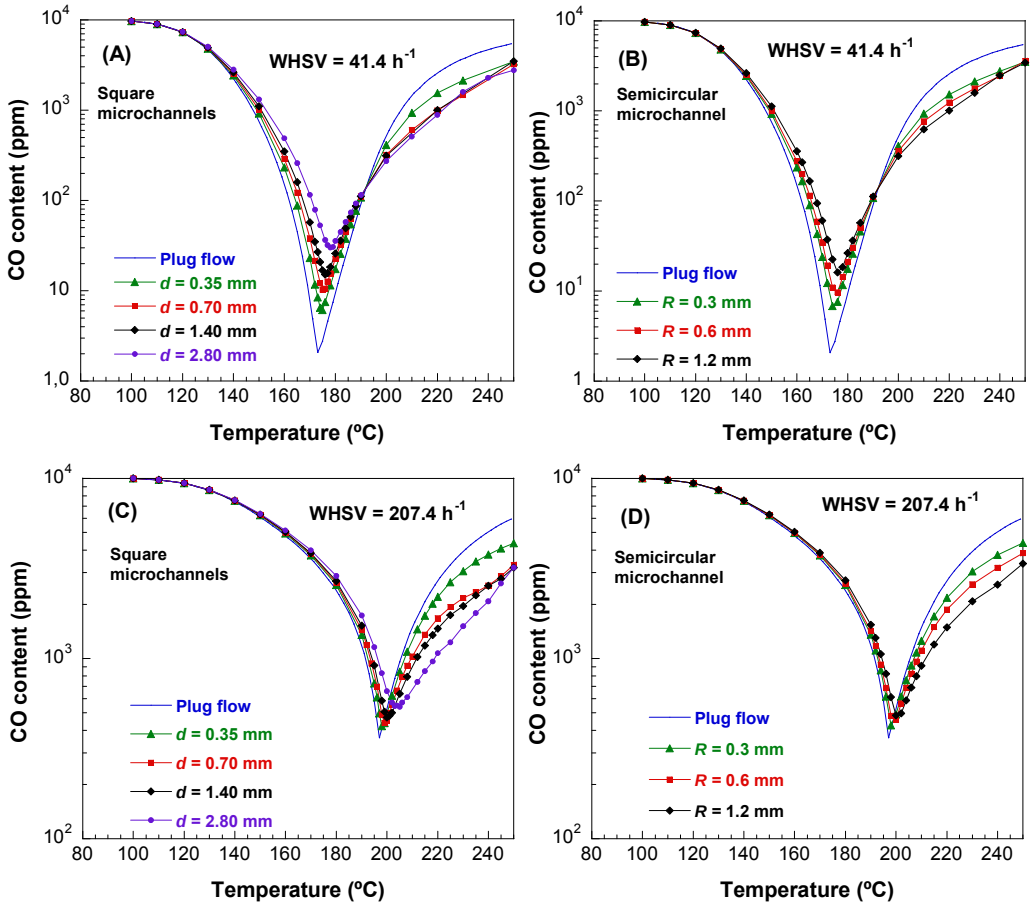

Fig. 5. Evolution of the mean CO content at the microreactor outlet as a function of the reaction temperature and the characteristic size of square (A,C) and semicircular (B,D) microchannels coated with the Au/CuO_x-CeO_2 catalyst (2 mg/cm^2). $\lambda = 4$.

The surface-to-volume ratio is inversely proportional to *d* or *R*. To take into account the change of the surface-to-volume ratio as the characteristic dimension varies, the results have been compared on the basis of the weight hourly space velocity (WHSV). This variable has been calculated as the total mass flow rate of the feed stream divided by the catalyst weight, which is given by the product of the inner walls surface area and the catalyst loading referred to the unit surface area. As a result, for a given WHSV, the space time is constant if the catalyst loading and feed stream composition are also constant, irrespective of the characteristic dimension and channel geometry. The results shown in Fig. 5 correspond to simulations performed with 2 values of the WHSV, 41.4 and 207.4 h^{-1} with a feed stream of composition corresponding to the base case (see Section 2). To give an idea, WHSV = 41.4 h^{-1} corresponds to GHSV = 10 000 h^{-1} in a square microchannel with d = 0.7 mm and catalyst loading of 2 mg/cm^2. On the other hand, WHSV = 207.4 h^{-1} is equivalent to GHSV = 50 000 h^{-1} in the same microchannel, and GHSV of 100 000 h^{-1} for d = 0.35 mm.

It is apparent according to Fig. 5 that the characteristic dimension affects the microreactor performance for CO-PROX as concerns the CO removal efficiency. In general, the mean CO content at the microchannels outlet increases with the increase of *d*. In the case of the square microchannels at WHSV = 41.4 h^{-1}, the minimum CO concentration increases from 5.7 to 10.2, 16.2 and 29 ppm as *d* increases from 0.35 to 0.7, 1.4 and finally 2.8 mm (Fig. 5A).The temperatures at which these concentrations area achieved increase slightly from 174 ºC for d = 0.35 mm to 178 ºC for d = 2.8 mm. As for the semicircular channels at WHSV = 41.4 h^{-1}, the minimum CO concentration increases from 6.9 to 9.9 and 16.2 ppm as *R* increases from 0.3 to 0.6 and 1.2 mm (Fig. 5B). As far as the surface-to-volume ratio is comparable, there are almost no differences between the square and semicircular channels. For example, 10.2 and 6.9 ppm of CO are present at the exit of the microchannels with d = 0.7 mm and R = 0.3 mm. The surface-to-volume ratios for these microducts are 5.7 and 5.4 mm^{-1}, respectively. The

results corresponding to the microchannels performance assuming plug-flow behavior, that is, the absence of transverse or radial concentration (and velocity) profiles, have been also included in Fig. 5. It can be seen that the minimum CO concentration under plug-flow regime is only 2.2 ppm at 173 ºC and WHSV of 41.4 h^{-1}. These results suggest that concentration profiles should develop as the characteristic dimension increases that negatively affect the CO oxidation rate and the reactor performance. Such profiles indeed exist although they are very smooth according to the CFD simulations. Nevertheless their effect is enough to produce changes of the CO concentration at the ppm level at the microreactor outlet. Previous results by our group for the steam reforming of methane in square microchannels and microslits with characteristic dimensions within the 0.35-2.8 mm range have shown the development of transverse concentration profiles for values of *d* above 0.7 mm leading to a decrease of the methane conversion [36]. In the case of CO-PROX, the reaction can be viewed as the competence between CO and H_2 for O_2. Moreover, under the laminar flow regime prevailing in the microchannels (maximum Reynolds number of about 5), these species should diffuse to the channels walls where the catalyst is located and the reactions take place. In the presence of stronger transport limitations as *d* increases, it can be expected that, due to its significantly higher diffusivity, the oxidation of H_2 becomes increasingly favored over that of CO. This would lead to a higher CO concentration at the reactor outlet in accordance with the simulation results.

As the space velocity increases to 207.4 h^{-1} (Figs. 5C and 5D) the exit CO concentration of the reformate increases, which is an obvious consequence of the lower residence time. Simulations corresponding to plug-flow regime predict a minimum CO content of 367 ppm at 197 ºC. Such a reformate would not be suitable for feeding a low-temperature PEMFC. In the case of the square microchannels, the minimum concentration of CO increases from 415, to 434, 462, and 538 ppm as *d* increases from 0.35 to 0.7, 1.4 and finally 2.8 mm (Fig. 5C).

These values are achieved at temperatures that slightly increase from 197 ºC for d = 0.35 mm to 204 ºC for d 0 2.8 mm. Regarding the semicircular microchannels, the minimum CO concentration increases from 415 to 455 and 498 ppm as R increases from 0.3 to 0.6 and 1.2 mm (Fig. 5D). In spite of the higher linear velocity compared with the cases at WHSV = 41.4 h^{-1}, the flow regime remains laminar (maximum Reynolds number of about 20) so the mass transport to the catalytic walls is also molecular diffusion-limited, thus explaining the effect of the increase of the characteristic size, as discussed above.

4. Non-isothermal simulations

Isothermal simulations have revealed that there is an optimal operating temperature at which the CO concentration of the reformate stream is reduced to a minimum value. As the oxidation reactions, particularly that of H_2, are very exothermic, controlling the reaction temperature through suitable cooling strategies is of the outmost importance for the CO-PROX process. In this work, this issue has been addressed considering 2 different cooling fluids: air and a mixture of 40 vol. % H_2 in N_2 that intends emulating in a simplified way the anode off-gas of a PEMFC. Both are interesting from the point of view of the thermal integration in complete fuel processor units to improve the energy efficiency of the system. For example, the anode off-gas can be recycled to a combustor where it reacts with air for supplying heat to the fuel reformer [2]. The combustion takes place at temperatures much higher than that of the CO-PROX reaction so, the anode off-gas, the air, or both, can be preheated cooling the CO-PROX reactor. Two inlet temperatures, 100 and 120 ºC, have been considered for the coolant stream. These values have been selected because they are close to that found in highly integrated portable fuel processors [16].

The physical model used in the non-isothermal CFD simulations consists in parallel square microchannels of side *d* (0.35, 0.7, 1.4 or 2.8 mm) and separated by the same distance *d*; the microreactor block is made of stainless steel and assumed adiabatic [32]. The flow of both the reformate and the cooling fluid was arranged as parallel cocurrent in channels of the same size with a feed stream of composition corresponding to the base case.

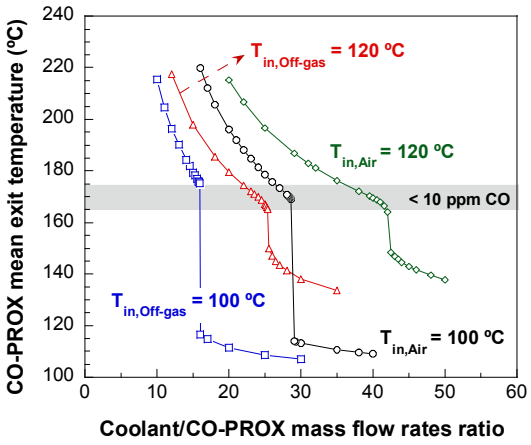

Fig. 6. Evolution of the mean CO-PROX reactor exit temperature as a function of the coolant (air or PEMFC anode off-gas surrogate) inlet temperature (100 or 120 ºC) and flow rate expressed as the ratio between the mass flow rates of the coolant and CO-PROX streams.

Fig. 6 shows the influence of the coolant inlet temperature and flow rate (expressed as the ratio between the mass flow rates of the coolant and CO-PROX streams) on the mean temperature at the reactor outlet. Simulations correspond to a reformate feed stream entering the reactor at 200 ºC and GHSV of 18 000 h^{-1}. The microchannels characteristic dimension was 0.7 mm and the catalyst (Au/CuO_x-CeO_2) loading 5 mg/cm^2. Under these conditions, the optimal operating temperature is 170ºC which leads to a minimum CO concentration of 4.2 ppm (see Fig. 3B). A shaded region has been included in Fig. 6 that corresponds to the 165-175 ºC range of temperatures at which the concentration of CO is reduced to less than 10 ppm. Depending on the coolant and its inlet temperature it may be necessary that the coolant mass flow rate is between 12 and 24 times higher than that of the CO-PROX feed stream in order to achieve that the temperature decreases from the entry value (200 ºC). The

flow rates are of course higher to reach the operating temperatures at which the exit CO concentration is below 10 ppm. To this end, the coolant mass flow rate should be 16 times higher than that of the CO-PROX feed stream when cooling is carried out with the anode off gas surrogate at 100 ºC, and up to 40 times higher when air entering the reactor at 120 ºC is used as the coolant. The required mass flow rate of coolant obviously increases as its inlet temperature also increases. On the other hand, for a given inlet temperature, the mass of coolant required is lower when the PEMFC anode off-gas surrogate is used due to its higher specific heat compared to that of air. Indeed, the mean specific heat of air under the simulation conditions is about 1 kJ/(kg ºC) whereas that of the H_2-N_2 mixture is 1.7 kJ/(kg ºC).

An interesting practical conclusion that can be drawn from the results in Fig. 6 is that the control of the reaction temperature will be more difficult if a relatively low coolant entry temperature is used. This is clearly seen for the case corresponding to cooling with the PEMFC anode off-gas surrogate at 100 ºC. A very small increase of the coolant flow rate with respect to the value leading to the optimal operating temperature may lead to an abrupt decrease of the reaction temperature to values as low as 115 ºC with the result of reaction extinction and the increase of the CO content of the reformate. In contrast, if the entry temperature is increased to 120 ºC, the effect of an accidental change of the coolant flow rate is much less important. Therefore, to improve the system stability and it is essential to carefully establish and control the coolant inlet temperature.

Fig. 7 shows the influence of the coolant (PEMFC anode off-gas surrogate at 120 ºC) to CO-PROX streams mass flow rates ratio and square microchannels characteristic dimension on the mean temperature and CO content at the reactor outlet. Simulations were performed at reformate WHSV of 29.9 h^{-1} that corresponds to GHSV 18 000 h^{-1} in microchannels with d = 0.7 mm and catalyst (Au/CuO_x-CeO_2) loading of 5 mg/cm^2.

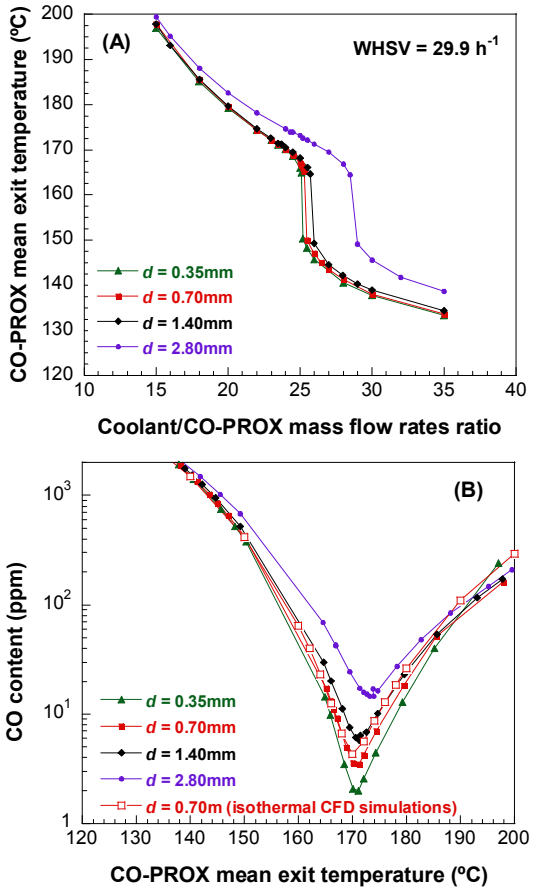

Fig. 7. Evolution of the mean CO-PROX reactor exit temperature (A) and mean CO content (B) as a function of the PEMFC anode off-gas surrogate to CO-PROX streams mass flow rates ratio and square microchannels characteristic dimension. Coolant inlet temperature = 120 ºC.

It can be seen in Fig. 7A that the required coolant mass flow rates required when using the highest characteristic dimension (2.8 mm) are much higher than for the rest of *d* values considered. This result evidences the loss of heat transfer efficiency of the microreactor that takes place as the characteristic dimension increases. On the other hand, as shown in Fig. 7B, the CO content of the reformate rapidly increases if the CO-PROX temperature decreases away from the region close to the optimum value. The CO concentration can easily exceed 100 ppm if the coolant flow rate increases accidentally and appropriate control actions are not adopted. Under the conditions of the simulations included in Fig. 7 there are no great behavior

differences as far as d is below 1.4 mm. However, for d = 2.8 mm, the microreactor is not capable of reaching 10 ppm or less of CO at the reactor exit.

An analysis of the temperature fields has shown that the temperature gradients within the microreactor block are very small so its behavior is almost isothermal. Indeed, it has been included in Fig. 7B the results of the isothermal CFD simulations for d = 0.7 mm (see Fig. 3B, GHSV = 18 000 h^{-1}). As can be seen, there are little differences between the results of the isothermal and non-isothermal simulations. The small characteristic dimensions of microreactors allow operating under close to isothermal conditions. This is of great interest for the CO-PROX reaction because it is possible to maintain the whole reactor virtually at the optimal temperature that leads to the minimal CO concentration in the reformate stream.

5. Conclusions

…

Acknowledgements

Financial support by the Spanish Ministry of Science and Innovation and Ministry of Economy and Competitiveness (ENE2009-14522-C04 and ENE2012-37431-C03 grants, respectively) is gratefully acknowledged. I. Uriz gratefully acknowledges the fellowships granted by the Innovation Department of the Navarre Government and the Spanish Ministry of Science and Innovation (program FPI, BES-2010-030021).

References

[1] A. Chandan, M. Hattenberger, A. El-kharouf, S. Du, A. Dhir, V. Self, B.G. Pollet, A. Ingram, W. Bujalski, J. Power Sources 231 (2013) 264-278.

[2] G. Kolb, Fuel Processing for Fuel Cells, Wiley-VCH, Weinheim, 2008.

[3] A. Qi, B. Peppley, K. Karan, Fuel Process. Technol. 88 (2007) 3-22.

[4] E.D. Park, D. Lee, H.C. Lee, Catal. Today 139 (2009) 280-290.

[5] G. Kolb, J. Schürer, D. Tiemann, M. Wichert, R. Zapf, V. Hessel, H. Löwe, J. Power Sources 171 (2007) 198-204.

[6] G. Kolb, C. Hofmann, M. O'Connell, J. Schürer, Catal. Today 147S (2009) S176-S184.

[7] M. O'Connell, G. Kolb, K.-P. Schelhaas, J. Schuerer, D. Tiemann, A. Ziogas, V. Hessel, Int. J. Hydrogen Energy 35 (2010) 2317-2327.

[8] G. Kolb, Chem. Eng. Process. 65 (2013) 1-44.

[9] N. Bion, F. Epron, M. Moreno, F. Mariño, D. Duprez, Top. Catal. 51 (2008) 76-88.

[10] G. Kolb, V. Hessel, V. Cominos, C. Hofmann, H. Löwe, G. Nikolaidis, R. Zapf, A. Ziogas, E.R. Delsman, M.H.J.M. de Croon, J.C. Schouten, O. de la Iglesia, R. Mallada, J. Santamaria, Catal. Today, 120 (2007) 2-20.

[11] I.-H. Son, W.-C. Shin, Y.-K. Lee, S.-C. Lee, J.-G. Ahn, S.-I. Han, H.-Jin kweon, J.-Y. Kim, M.-C. Kim, J.-Y. Park, J. Power Sources 185 (2008) 171-178.

[12] S.-M. Hwang, O.J. Kwon, S.H. Ahn, J.J. Kim, Chem. Eng. J. 149 (2009) 105-111.

[13] C. Galletti, S. Specchia, G. Sarocco, V. Specchia, Chem. Eng. J. 154 (2009) 246-250.

[14] O. Görke, P. Pfeifer, Int. J. Hydrogen Energy 36 (2011) 4673-4681.

[15] G. Neri, G. Rizzo, F. Corigliano, I. Arrigo, M. Caprì, L. De Luca, V. Modafferi, A. Donato, Catal. Today 147S (2009) S210-S214.

[16] E.R. Delsman, M.H.J.M. de Croon, A. Pierik, G.J. Kramer, P.D. Cobden, Ch. Hofmann, V. Cominos, J.C. Schouten, Chem. Eng. Sci. 59 (2004) 4795-4802.

[17] G. Guan, R. Zapf, G. Kolb, V. Hessel, H. Löwe, J. Ye, R. Zentel, Int. J. Hydrogen Energy 33 (2008) 797-801.

[18] G. Nikolaidis, T. Baier, R. Zapf, G. Kolb, V. Hessel, W.F. Maier, Catal. Today, 145 (2009) 90-100.

[19] H. Li, X. Yu, S.-T. Tu, J. Yan, Z. Wang, Appl. Catal. A: Gen. 387 (2010) 215-223.

[20] X. Yu, H. Li, S.-T. Tu, J. Yan, Z. Wang, Int. J. Hydrogen Energy 36 (2011) 3778-3788.

[21] C. Galletti, S. Specchia, G. Saracco, V. Specchia, Int. J. Hydrogen Energy 33 (2008) 3045-3048.

[22] P.V. Snytnikov, M.M. Popova, Y. Men, E.V. Rebrov, G. Kolb, V. Hessel, J.C. Schouten, V.A. Sobyanin, Appl. Catal. A: Gen. 350 (2008) 53-62.

[23] I. López, T. Valdés-Solís, G. Marbán, Int. J. Hydrogen Energy 33 (2008) 197-205.

[24] S.H. Zeng, Y. Liu, Appl. Surf. Sci. 254 (2008) 4879-4885.

[25] D.I. Potemkin, P.V. Snytnikov, V.D. Belyaev, V.A. Sobyanin, Chem. Eng. J. 176-177 (2011) 165-171.

[26] O.H. Laguna, E.M. Ngassa, S. Oraá, A. Álvarez, M.I. Domínguez, F. Romero-Sarria, G. Arzamendi, L.M. Gandía, M.A. Centeno, J.A. Odriozola, Catal Today 180 (2012) 105-110.

[27] Q. Zhang, L. Shore, R.J. Farrauto, Int. J. Hydrogen Energy 37 (2012) 10874-10880.

[28] O.H. Laguna, M.I. Domínguez, S. Oraá, A. Navajas, G. Arzamendi, L.M. Gandía, M.A. Centeno, M. Montes, J.A. Odriozola, Catal Today 203 (2013) 182-187.

[29] O. Goerke, P. Pfeifer, K. Schubert, Appl. Catal. A 263 (2004) 11-18.

[30] E. Lopez, G. Kolios, G. Eigenberger, Chem. Eng. Sci. 62 (2007) 5598-5601.

[31] N.J. Divins, E. López, M. Roig, T. Trifonov, A. Rodríguez, F. González de Rivera, L.I. Rodríguez, M. Seco, O. Rossell, J. Llorca, Chem. Eng. J. 167 (2011) 597-602.

[32] G. Arzamendi, I. Uriz, P.M. Diéguez, O.H. Laguna, W.Y. Hernández, A. Álvarez, M.A. Centeno, J.A. Odriozola, M. Montes, L.M. Gandía, Chem. Eng. J. 167 (2011) 588-596.

[33] O.H. Laguna, W.Y. Hernández, G. Arzamendi, L.M. Gandía, M.A. Centeno, J.A. Odriozola, Int. J. Hydrogen Energy (submitted).

[34] G. Arzamendi, P.M. Diéguez, M. Montes, M.A. Centeno, J.A. Odriozola, L.M. Gandía, Catal. Today 143 (2009) 25-31.

[35] G. Arzamendi, P.M. Diéguez, M. Montes, J.A. Odriozola, E. Falabella Sousa-Aguiar, L.M. Gandía, Chem. Eng. J. 154 (2009) 168-173.

[36] I. Uriz, G. Arzamendi, E. López, J. Llorca, L.M. Gandía, Chem. Eng. J. 167 (2011) 603-609.

[37] G. Arzamendi, I. Uriz, A. Navajas, P.M. Diéguez, L.M. Gandía, M. Montes, M.A. Centeno, J.A. Odriozola, AIChE J. 58 (2012) 2785-2797.

Captions

Table 1 Estimated kinetic parameters of the rate equations for the CO-PROX over Au/CuO_x-CeO_2 catalyst.

Fig. 1. Evolution of the mean CO content (A), O_2 conversion (B), CO conversion (C) and H_2 conversion (D) at the microchannels (d = 0.7 mm) outlet as a function of the reaction temperature for the base case CO-PROX over the catalysts indicated. GHSV=10 000 h^{-1}, 1 vol. % CO, $\lambda = 4$, and catalyst loading of 1 mg/cm^2.

Fig. 2. Evolution of the mean CO content (A) and the hydrogen conversion (B) at the microchannels (d = 0.7 mm) outlet as a function of the reaction temperature and the oxygen-to-CO ratio. GHSV = 10 000 h^{-1}, catalyst loading of 1 mg/cm^2. Open symbols: Au/CuO_x-CeO_2 catalyst; filled symbols: CuO_x-CeO_2 catalyst.

Fig. 3. Evolution of the mean CO content at the microchannels (d = 0.7 mm) outlet as a function of the reaction temperature and the catalyst loading (A) and GHSV (B). $\lambda = 4$. Open symbols: Au/CuO_x-CeO_2 catalyst; filled symbols: CuO_x-CeO_2 catalyst.

Fig. 4. Evolution of the mean CO content at the microchannels (d = 0.7 mm) outlet as a function of the reaction temperature and the CO_2 concentration for the microreactor coated with the Au/CuO_x-CeO_2 catalyst (2 mg/cm^2). GHSV=10 000 h^{-1}, $\lambda = 2$.

Fig. 5. Evolution of the mean CO content at the microreactor outlet as a function of the reaction temperature and the characteristic size of square (A,C) and semicircular (B,D) microchannels coated with the Au/CuO_x-CeO_2 catalyst (2 mg/cm^2). $\lambda = 4$.

Fig. 6. Evolution of the mean CO-PROX reactor exit temperature as a function of the coolant (air or PEMFC anode off-gas surrogate) inlet temperature (100 or 120 ºC) and flow rate expressed as the ratio between the mass flow rates of the coolant and CO-PROX streams.

Fig. 7. Evolution of the mean CO-PROX reactor exit temperature (A) and mean CO content (B) as a function of the PEMFC anode off-gas surrogate to CO-PROX streams mass flow rates ratio and square microchannels characteristic dimension. Coolant inlet temperature = 120 ºC.

Table 1. Estimated kinetic parameters of the rate equations for the CO-PROX over Au/CuO_x-CeO_2 catalyst. [a]

Parameter	Value
k_{CO}^{ref} [mol/(s·$g_{cat.}$·$atm^{1.5}$)]	4.15
E_{CO} [kJ/mol]	30.0
$K_{CO_2}^{ref}$ [atm^{-1}]	$1.12 \cdot 10^{3}$
$(-\Delta H)_{CO_2}$ [kJ/mol]	79.8
$K_{O_2}^{ref}$ [$atm^{-0.5}$]	145.1
$(-\Delta H)_{O_2}$ [kJ/mol]	0.3
$k_{H_2}^{ref}$ [mol/(s·$g_{cat.}$·$atm^{1.5}$)]	$2.1 \cdot 10^{-6}$
E_{H_2} [kJ/mol]	110.1
k_{RWGS}^{ref} [mol/(s·$g_{cat.}$·atm^{2})]	$5 \cdot 10^{-9}$
E_{RWGS} [kJ/mol]	36.9

[a] Values of the kinetic and adsorption equilibrium constants are given at 373 K.

Table 1.